Object Detection and Classification in Aerial Hyperspectral Imagery using a Multivariate Hit-or-Miss Transform

Fraser Macfarlane[a], Paul Murray[a], Stephen Marshall[a] and Henry White[b]

[a]Department of Electronic & Electrical Engineering, University of Strathclyde, Glasgow, Scotland

[b]BAE Systems, Air Sector, Filton, Bristol, UK

ABSTRACT

High resolution aerial and satellite borne hyperspectral imagery provides a wealth of information about an imaged scene allowing for many earth observation applications to be investigated. Such applications include geological exploration, soil characterisation, land usage, change monitoring as well as military applications such as anomaly and target detection. While this sheer volume of data provides an invaluable resource, with it comes the curse of dimensionality and the necessity for smart processing techniques as analysing this large quantity of data can be a lengthy and problematic task. In order to aid this analysis dimensionality reduction techniques can be employed to simplify the task by reducing the volume of data and describing it (or most of it) in an alternate way. This work aims to apply this notion of dimensionality reduction based hyperspectral analysis to target detection using a multivariate Percentage Occupancy Hit or Miss Transform that detects objects based on their size shape and spectral properties. We also investigate the effects of noise and distortion and how incorporating these factors in the design of necessary structuring elements allows for a more accurate representation of the desired targets and therefore a more accurate detection. We also compare our method with various other common Target Detection and Anomaly Detection techniques.

Keywords: Hyperspectral image processing, Mathematical morphology, Hit-or-Miss Transform, Template matching, Object detection

1. INTRODUCTION

Object detection from airborne imagery is, and continues to be, a major challenge and active area of research within the disciplines of signal and image processing. Remote sensing has become more and more prevalent and remains an important source of information in determining land usage, earth mapping and other similar areas of research. Depending on the system, remote sensing data can consist of high resolution RGB data, radar or multispectral or hyperspectral images. The latter, while providing a great deal of useful information about the scene it captures, introduces a vast quantity of data which must be handled and processed. The detection of objects within this multi-source data can be challenging and general techniques that can be readily applied to multiple sources are of great benefit.

A Multi-Dimensional Percentage Occupancy Hit-or-Miss Transform (MDPOHMT)[1] has been developed as an extension of the traditional Mathematical Morphology (MM) operation the Hit-or-Miss Transform (HMT) to multivariate images. This allows for targets to be detected in colour and multivariate images based on their size, shape and colour or spectral information. Whilst the initial aim of this work was the extension to colour images, the nature of the extension meant it would work well for higher dimensional images such as multi-spectral or hyperspectral images given some other initial preprocessing stages. This work was explored previously[2] but was only concerned with our method tested on a single dataset. In this paper we present a more in-depth evaluation of this extension of the MDPOHMT, we also investigate its use for target detection in hyperspectral imagery compared with other common target and anomaly detection techniques. We compare various techniques over multiple datasets in order to assess the performance of the MDPOHMT as a target detection algorithm.

This paper is structured as follows, section 2 gives an overview of related work and background information of various target and anomaly detection schemes, section 3 describes our MDPOHMT and various processing

Further author information: E-mail: fraser.macfarlane@strath.ac.uk

steps to improve its accuracy and efficiency when using hyperpsectral data. In section 4 we present our results from these techniques on aerial hyperspectral data and sections 5 and 6 contain our conclusions and future work respectively.

2. RELATED WORK

Generally object detection can be attributed to one of two main subcategories.[3] In target detection (TD), some prior information abut the desired targets is known and is provided to the detection method. Conversely, in an anomaly detection (AD) approaches, prior information is either unknown or not supplied to the detection algorithm, objects are detected on the basis of being irregular when compared to their surroundings, a comparison which can be performed globally or locally within an image. TD algorithms can be further categorised as structured or unstructured,[4] where structured methods rely on the underlying assumption that any pixel is made up of varying abundances of a set of constituent endmember spectra whereas unstructured approaches describe pixels in terms of their probability distributions. AD applications generally depend on anomalous pixels being outliers, differentiable from their surroundings as well as occurring with low probability.[5] Other methods based on finding or estimating endmembers as well as spectral comparisons are often used within TD and AD.

2.1 Target detection

There are many target detection algorithms available in literature and it is an ever growing and improving area of research, one widely used method is Constrained Energy Minimisation (CEM).[6] CEM is an FIR linear filter based approach that seeks to minimise the output energy of the filter when some desired target spectra, d, is input. The task of a CEM detector is to minimise the set of weighting coefficients of the filter and due to this underlying reliance on d, CEM is very susceptible to noise and can only detect pure forms of d. CEM can sometimes struggle to pick out the desired spectra in a mixed pixel or to differentiate it from spectra that are similar.[7] The Adaptive Cosine/Coherent Estimator (ACE)[8] is another method commonly used in hyperspectral target detection.[9,10] ACE works by computing the cosine of the angle between a zero-mean pixel and zero-mean target spectra in a whitened space, or one which has covariance equal to the identity matrix. The ACE statistic is a measure of the likelihood that this pixel contains a target of interest.

Other TD algorithms such as the Orthogonal Subspace Projection (OSP), Generalised Likelihood Ratio Test (GLRT) and Adaptive Matched Subspace Detector (AMSD) require prior knowledge of the background spectra which may not always be known in TD applications. These methods are intended to be investigated further in the future however in this paper, the use of ACE and CEM are investigated.

2.2 Anomaly Detectors

The Reed-Xiaoli Detector (RXD)[11] was developed by Reed and Yu in 1990 and is often considered the benchmark algorithm for AD in hyperspectral data.[3] The RXD can be thought of as the opposite of Principal Component Analysis (PCA), where PCA decorrelates data and attempts to compress the most significant information into few components. RXD seeks to seeks to find samples which occur with low probability in minor components.[6] An issue with the RXD is that it cannot differentiate between small, low probability objects and noise. This, however, does not reduce its ability to detect other outliers.

2.3 Endmember Finders

Another useful set of tools for object detection in hyperspectral imagery are endmember extraction, or unmixing, algorithms. Some commonly used unmixing algorithms are the Sequential Maximum Angle Convex Cone (SMACC),[12] Automatic Target Generation Process (ATGP),[13] Vertex Component Analysis (VCA)[14] and Independent Component Analysis - Endmember Extraction Algorithm (ICA-EEA).[15] Each of these methods seek to find the endmember pixels that are combined in varying abundances to create the full image. Once these endmembers have been found, further processing can determine if pixels are outliers with the latter three of these methods are reviewed for unmixing in.[16]

2.4 Spectral Comparison

In some cases, a direct comparison between image spectra and the desired spectra d is sufficient to determine whether the pixel under test (PUT) contains d. Two common comparisons are the Spectral angle mapper (SAM)[17] and Spectral information divergence (SID).[18] Both work in similar ways by drawing comparisons between two N-dimensional pixel vectors x_i and x_j with SAM simply being the angle between the two. SID is a measure of band-band variability between two vectors derived from the Kullback-Leibler information measure[6] and uses the relative entropy between x_i and x_j to calculate their similarity. Combining both SAM and SID using tan and sin functions has been shown to improve both measures.[19]

2.5 Morphological Techniques

MM is a fundamental set of image processing techniques used for image analysis and classification first introduced by Matheron[20] and Serra.[21] In the decades since its inception MM has undergone many successive extensions from its initial restrictions to use in binary images.[22,23] The HMT is a common MM technique used for detecting objects based on their size and shape information and does this by probing a query image with two structuring elements (SEs). These SEs should be designed to detect objects by fulfilling both of the following conditions, one SE, the foreground SE, must match the foreground and the other, the background SE, the complement of background. In the binary case this is equivalent to basic set theory operations and can be implemented using Erosions and Dilations.[24] The erosion of an image, I, by an SE S (ϵ_S), is the locus of all points in an image where S can fit entirely within the image foreground. The dilation of I by S (δ_S), is the locus of all points where S touches, or intersects, the foreground. Alternatively, erosions can be thought of as being minimum filters within the region bounded by S and conversely, dilations maximum filters. The HMT of I can be defined in terms of an erosion of the foreground and a dilation of the background with a composite SE S, with $S = [S_{FG}, S_{BG}]$ where $S_{FG} \cap S_{BG} = \varnothing$.

$$[\mathrm{HMT_S}(X)](\mathbf{x}) = \begin{cases} 1, & \text{if } [\delta_{S_{\mathrm{BG}}}](\mathbf{x}) < [\varepsilon_{S_{\mathrm{FG}}}](\mathbf{x}) \\ 0, & \text{otherwise} \end{cases} \tag{1}$$

There have been various efforts to extend MM and the HMT to greyscale images and beyond. A unified theory now exists for the greyscale HMT[25] however, no such unified theory exists for a further colour or multivariate extension and various proposed methods exist in literature.[26–30]

3. THE MDPOHMT AS A TARGET DETECTION ALGORITHM

3.1 Multivariate Mathematical Morphology using a MDPOHMT

The main difficulty in extending MM to multivariate images comes from the underlying need to define a complete lattice[31] or totally ordered set for morphological operations to be implemented. The idea of a total order in a multivariate space is not intuitive, however, there are multiple methods[32] to circumvent this. One of these such methods, reduced ordering or r-ordering, is used in the MDPOHMT. R-ordering takes vectorial data and reduces its dimension by measuring the dissimilarity from some reference which is a scalar. These scalar valued representations of the vectorial data can then be ordered and morphological operations can be defined. The measure used in the MDPOHMT is the Euclidean distance in the RGB colour space however many other common distance measures and colour spaces can be used. The normalised Euclidean distance, $\hat{d}$, between two N-dimensional pixel vectors a and b is

$$\hat{d}(a,b) = \frac{\sqrt{(b_1 - a_1)^2 + (b_2 - a_2)^2 + ... + (b_N - a_N)^2}}{\sqrt{N}} \tag{2}$$

Using this Euclidean distance or another similar measure allows for the definition or r-ordering based erosion, dilation and rank-order filters, which erosion and dilation are special cases of:

$$[\varepsilon_S(D)](x) = \min_{s \in S} \hat{d}(I(x+s), S(s)) \tag{3}$$

$$[\delta_S(D)](x) = \max_{s \in S} \hat{d}(I(x+s), S(s)) \tag{4}$$

$$[\xi_{S,k}(D)](x) = k\text{th} \underset{s \in S}{\text{rank}}\{\hat{d}(I(x+s), S(s))\} \tag{5}$$

Using the distance-based definition of k$^{\text{th}}$ rank order filters from (5) and combining two of them, one in the foreground and another in the background using a composite SE, S, similar to that used in (1), a definition for the MDPOHMT of an image I can be reached,

$$[\text{MDPOHMT}_S(I)](x) = \begin{cases} 1 & \text{if } [\xi_{S_{FG},k_{100-p}}(D)](x) < [\xi_{S_{BG},k_p}(D)](x) \\ 0, & \text{otherwise} \end{cases} \tag{6}$$

Where $[\xi_{S_{FG},k_{100-p}}(D)](x)$ and $[\xi_{S_{BG},k_p}(D)](x)$ are relaxed distance based erosion and dilation by S_{FG} and S_{BG} respectively.

3.2 Dimensionality Reduction

Our proposed method combines the spatial and spectral/colour analysis provided by using an MDPOHMT with various spatial and spectral dimensionality reduction (DR) techniques. By using DR, the efficiency of the process is increased. As the HMT requires SEs in order to detect objects of interest, the SEs have to be projected into the same reduced domain as the image. Principal component analysis (PCA)[33] and its variants offer a method of projecting auxiliary, or supplementary, variables which were not present during the calculation of the principal components into the same reduced domain using a coefficient or projection matrix. This allows for the image and associated SEs to be projected into the same reduced domain by the image's principal component coefficient matrix, Q, for processing as show in equations (7) and (8):

$$\hat{X} = X \cdot Q \tag{7}$$

$$\hat{X}_{\text{SE}} = X_{\text{SE}} \cdot Q \tag{8}$$

Where X and X_{SE} are the image and SE respectively and $\hat{X}$ and $\hat{X}_{\text{SE}}$ are their projections.

While PCA is an optimal set of compression coefficients, it is not the most practical method as it is calculated on a per-image basis, so part of the investigation was finding a set of coefficients for a set of images that was representative enough to only be calculated for one, or multiple, image(s) from the set. By projecting each image and the corresponding set of SEs using one set of representative coefficients, a more efficient process is defined. The proposed method is shown graphically in Figure 1 while a flowchart of the proposed methods is shown in Figure 2.

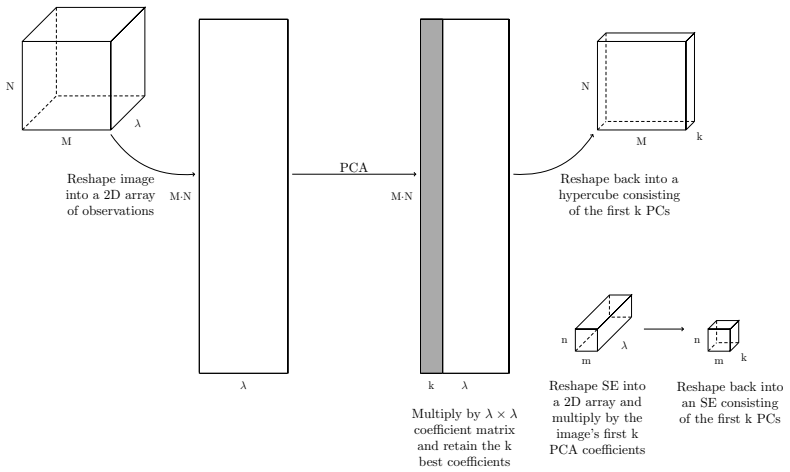

Figure 1: Proposed dimensionality reduction scheme using PCA to project an image and any relevant SEs into the same reduced-dimension domain.

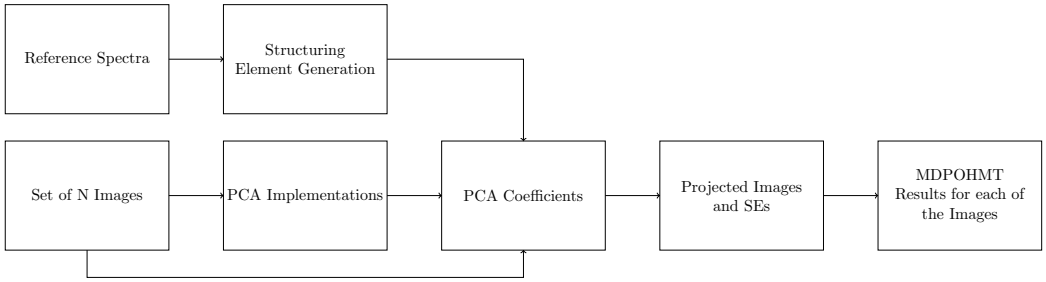

Figure 2: Flowchart of the proposed method for spectral dimensionality reduction for a set of images and their SEs.

PCA and its variants, along with many other forms of DR seek to exploit spectral redundancy. With large hyperspectral images this is desirable to overcome the so called curse of dimensionality. However, spatial redundancy is often exhibited in remote sensing applications and target/anomaly detection, wherein much of the image is vegetative. Using spatial measures such as the Normalised Difference Vegetation Index, or NDVI, pixels containing large amounts vegetation can identified. NDVI is a simple and effective technique in determining the amount of vegetation present in each pixel. The intensities at two wavelengths are used to obtain a ratio that determines the NDVI, one in the red part of the spectrum, λ_{RED}, where it is absorbed by vegetation and another in the Near-IR, λ_{NIR}, where it is reflected. using these wavelengths the NDVI is calculated as:

$$\text{NDVI} = \frac{\lambda_{\text{NIR}} - \lambda_{\text{RED}}}{\lambda_{\text{NIR}} + \lambda_{\text{RED}}} \tag{9}$$

The values of the NDVI can be thresholded and used to mask out regions of interest in the image, reducing the number of PUT to be queried using the MDPOHMT. Larger values indicate a higher likelihod that the pixel contains vegetation. The stages of this NDVI segmentation are shown in Figure 3. NDVI coupled with spectral DR results in speed increases on some images, as found in our previous study.[2] The DR techniques used also has the added advantage of increasing the accuracy of target detection due to the targets high variance being accentuated by PCA.

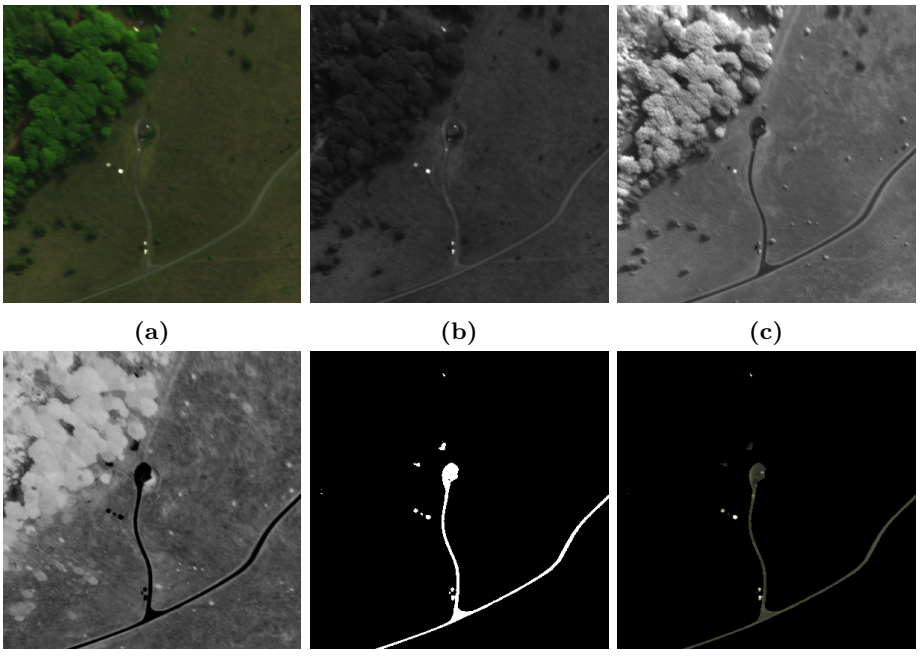

Figure 3: Stages of NDVI segmentation: a) Pseudo-colour image of the OP7 Site b) RED IMAGE c) NIR IMAGE d) NDVI measurement of the scene e) Thresholded image specifying synthetic ROI f) Masked pseudo-colour image

3.3 Noise Robustness

Robustness to various noise and occlusion effects can be realised in multiple ways. Occlusion, dead pixel and salt-and-pepper noise like effects can be negated using Percentage Occupancy[34] in the MDPOHMT. This allows for the SEs to have some disparity in their size and shape when compared with query regions within the image. Atmospheric attenuation and noise can sometimes be observed in high altitude imagery and can adversely affect template based object detection. Such noise can be modelled and their effects applied to the ground truth spectra, such that this ground truth is altered in the same way as the scene upon capture. By combining this noise robustness with the spatial robustness afforded by percentage occupancy the MDPOHMT can be made more robust to noise.

4. EXPERIMENTAL RESULTS

4.1 Image Acquisition

Images from multiple sources have been used to validate the techniques described here. The first, provided by BAE Systems, were acquired on the 18th May 2014 from an aerial platform flying at approximately 0.78km. The platform used a hyperspectral sensor with a spectral range of roughly 400 - 1000nm. The second set of images are taken from the MUULF Gulfport Dataset[35] and include four 6×10m atmospheric calibration panels as well as 60 other targets ranging from 0.5×0.5m sub-pixel targets to 3×3m targets. The sensor used was the Compact Airborne Spectrographic Imager (CASI-1500) which has a spatial resolution of 1m with a spectral range of roughly 360-1040nm.The images were captured from 1km and 2km altitudes on the 8th November 2010. Examples from these datasets can be seen in Figures 1 and 2 respectively.

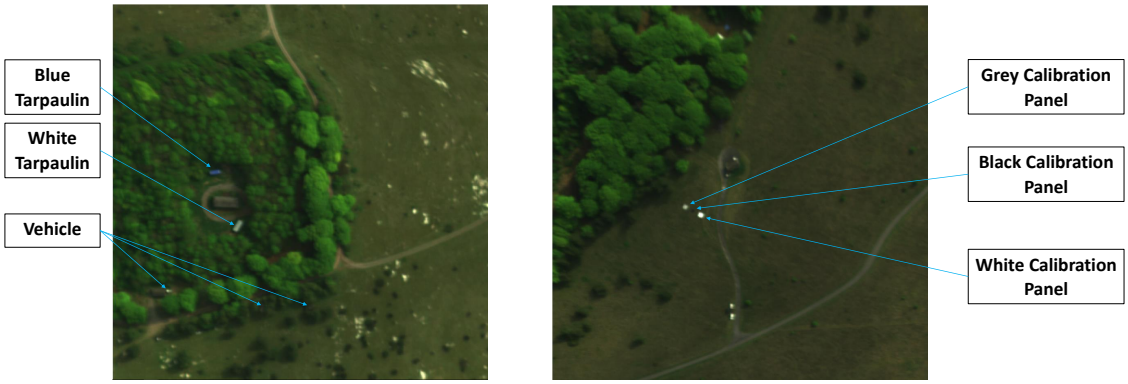

Figure 4: Examples of data provided by BAE Systems - both of which show various objects in forested areas, a) Image from the Moll Harris dataset, b) Image from the Operation 7 dataset.

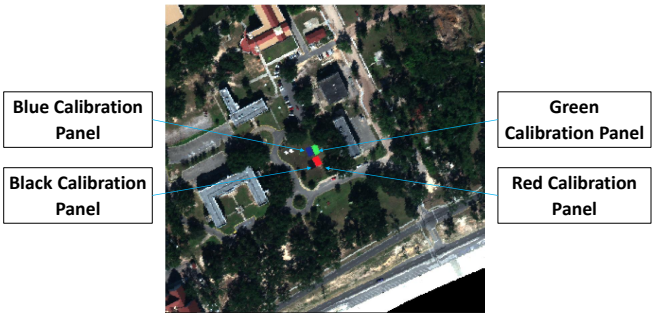

Figure 5: Image from the MUUFL Gulfport dataset.

4.2 MDPOHMT with added dimensionality reduction

Initially, the effects of the DR added to the MDPOHMT were tested using the images from the OP7 dataset supplied by BAE systems. Each of these images showed the same scene with three atmospheric calibration panels in the open along with other objects in the scene. The spectra of each of these panels was known and appropriate SEs were designed and the MDPOHMT was used to detect the objects with PCA and NDVI applied to the image. The resultant timings for each method are shown in Table 1 and in the bar chart in Figure 6. The results of the algorithm and its added DR schemes can be seen in Figure 7.

Table 1: Comparison of execution time and effects of each DR method on the OP7 dataset.

Pre-processing	Raw	PCA	NDVI	PCA + NDVI
Average Time (s)	124.1903	7.6360	2.2747	**0.1383**
No. Pixels retained	16800000	480000	319410	12168
% of Total Pixels	100%	2.8571%	1.9013%	0.0730%

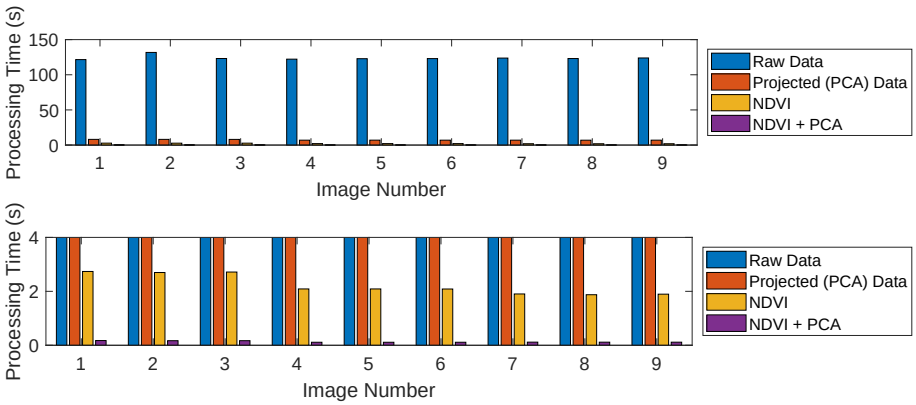

Figure 6: Execution time of the MDPOHMT with the various DR techniques - the lower graph is magnified focussing the bottom of the first.

As expected, analysing the image with the spectral DR afforded by PCA the run-time of the MDPOHMT is greatly reduced in comparison to the raw image. Applying both NDVI and PCA further improves the run-time. The effects of these DR techniques on the accuracy of the HMT are shown in Table 2 where each technique is assessed in terms of their precision, based on the resulting true and false positives.

Table 2: Comparison of the precision accuracy and F1 Score of each HMT on the OP7 dataset.

Pre-processing	Raw	PCA	NDVI	PCA + NDVI
True Positives	9	9	9	9
False Positives	679	11	23	5
Precision	0.0234	0.3529	0.2813	0.6429
Accuracy	0.0384	0.5769	0.3947	0.75
F1 Score	0.0458	0.6207	0.4390	0.7826

The precision of the HMT increases as the false positives in the original image are reduced. This reduction can be attributed to the masking of the areas of interest through NDVI as well as the variance exaggeration and projection of PCA.

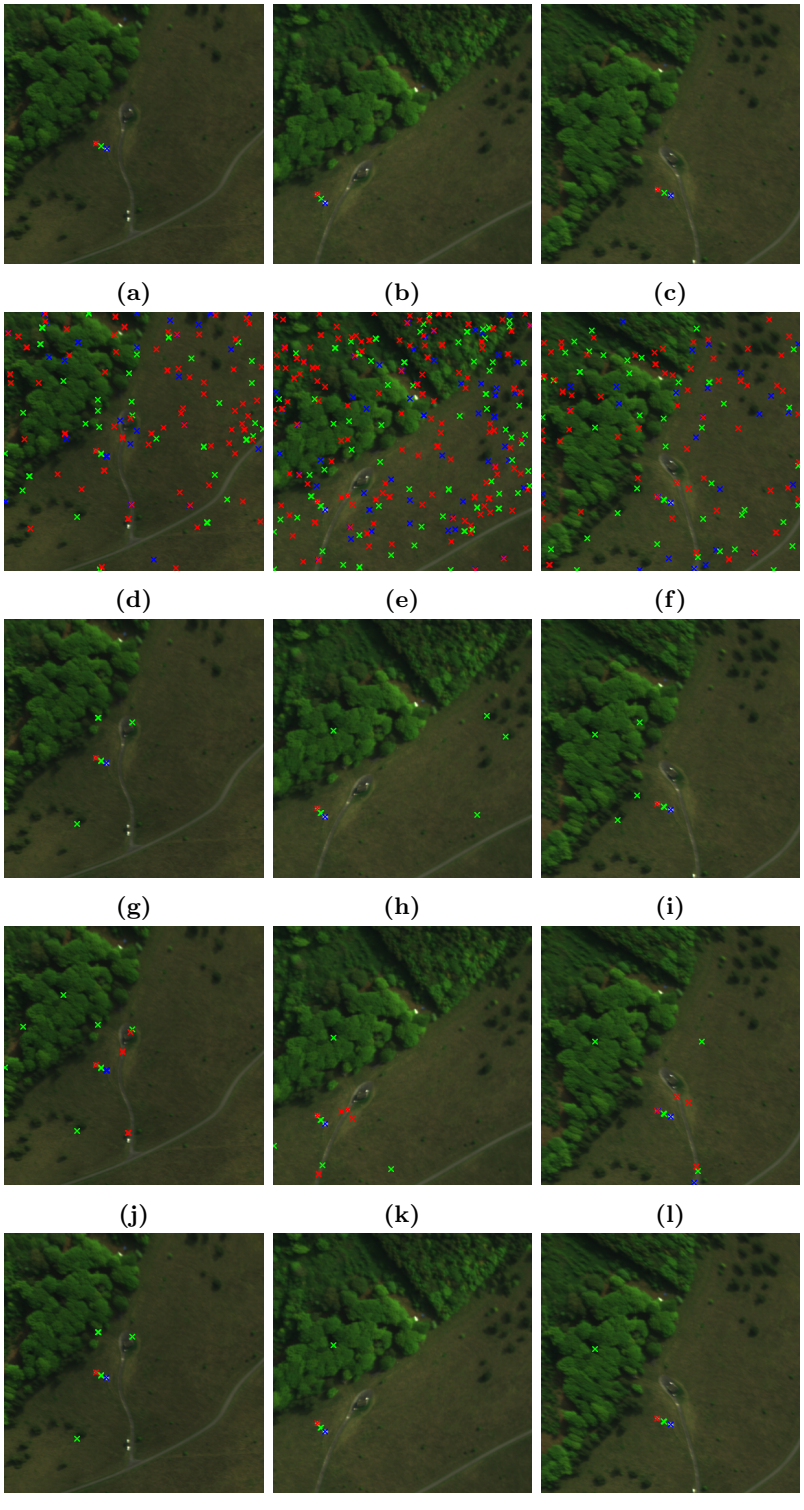

Figure 7: Results of the dimensionality reduction on the MDPOHMT a-c) Ground truth locations, d-f) Results of the raw MDPOHMT, g-i) Results of the MDPOHMT with PCA applied, j-l) Results of the MDPOHMT with NDVI applied, m-o) Results of the MDPOHMT with both PCA and NDVI applied.

4.3 Comparison between the MDPOHMT and other common TD/AD methods

The MDPOHMT was then applied with other common TD and AD methods, these were ACE, CEM, RXD, SAM and SID and their performance on two datasets were recorded. These methods were chosen as they and their variants are still widely used in similar target detection applications[10,36–39]

The first dataset these methods were tested on, the MUUFL Gulfport dataset (Figure 5), comprised of 3 images, each with 4 atmospheric calibration panels prominent within the scene as well as various other assorted targets. These four calibration tiles were correctly detected within each of the images using each of the methods and the results are collated in Table 3:

Table 3: Comparison of the pixel-wise target detection of each algorithm

Algorithm	MDPOHMT (NDVI+PCA)	ACE	CEM	SAM	SID	RXD
Targets Detected	12	12	12	12	12	12
Targets Missed	0	0	0	0	0	0
Time taken (s)	0.2451	0.2152	0.1312	0.2308	3.7186	0.1791

The Moll-Harris dataset provided by BAE Systems (Figure 4a) consisted of an image with two targets in a woodland clearing as well as three partially concealed vehicles. The targets in this image were objectively more difficult to find than the ones attempted in the previous experiment as there were partially concealed and camouflaged vehicles. Each method was tested in its ability to detect these five objects and the results are displayed in Table 4:

Table 4: Comparison of the pixel-wise target detection of each algorithm

Algorithm	MDPOHMT (NDVI+PCA)	ACE	CEM	SAM	SID	RXD
Targets Detected	5	4	3	4	5	4
Targets Missed	0	1	2	1	0	1
Time taken (s)	0.8478	0.7912	0.1332	0.3969	5.0502	0.6908

The MDPOHMT and SID based approaches successfully detected all five objects whilst the other methods missed either one or two of the concealed vehicles. Of the two methods to detect all five objects SID had the longer running time whilst the MDPOHMT performed much quicker. The CEM scheme was the quickest of all of those tested but had the worst detection rate whilst ACE and SAM both worked well but failed to detect a camouflaged object.

5. CONCLUSION

We have presented an extension of the morphological Hit-or-Miss transform the MDPOHMT for use in hyperspectral and other multivariate imagery.We have also investigated its use as a target detection algorithm and compared it with other commonly used target and anoaly detection techniques. While the algorithm works well when used on both raw and dimensionality reduced images, it requires several pure spectral pixels on target or for mixed spectra containing the target to be known or estimated. This shortcoming is present in many of the TD algorithms explored here.

6. FUTURE WORK

While both PCA and NDVI have been implemented to positive effect, other DR techniques may also prove useful. Mutual information based band selection may also be used and also allows for any relevant SEs to remain in the same domain as any images. Using the Euclidean distance as a disparity measure is related to the SAM metric[6] and at its heart the MDPOHMT can be classed as an extended variant of a distance-based measure of spectral comparison. Given this, other spectral comparisons such as SAM or SID may be incorporated into the MDPOHMT in hyperspectral applications and may be a more relevant discrimination metric in these scenarios.

ACKNOWLEDGMENTS

The authors would like the thank the EPSRC and BAE Systems for providing the funding necessary to carry out this work. The authors would also like to thank BAE Systems for providing the data used in this work.

REFERENCES

[1] Macfarlane, F., Murray, P., Marshall, S., Perret, B., Evans, A., and White, H., "A colour hit-or-miss transform based on a rank ordered distance measure," in [*2018 26th European Signal Processing Conference (EUSIPCO)*], 588–592 (2018).

[2] Macfarlane, F., Murray, P., Marshall, S., and White, H., "A fast hyperspectral hit-or-miss transform with integrated projection-based dimensionality reduction," in [*Hyperspectral Imaging HSI*], (2018).

[3] Matteoli, S., Diani, M., and Corsini, G., "A tutorial overview of anomaly detection in hyperspectral images," *IEEE Aerospace and Electronic Systems Magazine* **25**(7), 5–28 (2010).

[4] Cisz, A. P. and Schott, J. R., "Performance comparison of hyperspectral target detection algorithms in altitude varying scenes," in [*Algorithms and Technologies for Multispectral, Hyperspectral, and Ultraspectral Imagery XI*], **5806**, 839–850, International Society for Optics and Photonics (2005).

[5] Guo, Q., Pu, R., and Cheng, J., "Anomaly detection from hyperspectral remote sensing imagery," *Geosciences* **6**(4), 56 (2016).

[6] Chang, C.-I., [*Hyperspectral imaging: techniques for spectral detection and classification*], vol. 1, Springer Science & Business Media (2003).

[7] Ren, H., Du, Q., Chang, C.-I., and Jensen, J. O., "Comparison between constrained energy minimization based approaches for hyperspectral imagery," in [*IEEE Workshop on Advances in Techniques for Analysis of Remotely Sensed Data, 2003*], 244–248, IEEE (2003).

[8] Scharf, L. L. and McWhorter, L. T., "Adaptive matched subspace detectors and adaptive coherence estimators," in [*Conference Record of the Thirtieth Asilomar Conference on Signals, Systems and Computers*], 1114–1117, IEEE (1996).

[9] Pieper, M., Manolakis, D., Lockwood, R., Cooley, T., Armstrong, P., and Jacobson, J., "Hyperspectral detection and discrimination using the ace algorithm," in [*Imaging Spectrometry XVI*], **8158**, 815807, International Society for Optics and Photonics (2011).

[10] Gao, L., Yang, B., Du, Q., and Zhang, B., "Adjusted spectral matched filter for target detection in hyperspectral imagery," *Remote Sensing* **7**(6), 6611 (2015).

[11] Reed, I. S. and Yu, X., "Adaptive multiple-band cfar detection of an optical pattern with unknown spectral distribution," *IEEE Transactions on Acoustics, Speech, and Signal Processing* **38**(10), 1760–1770 (1990).

[12] Gruninger, J. H., Ratkowski, A. J., and Hoke, M. L., "The sequential maximum angle convex cone (smacc) endmember model," in [*Algorithms and technologies for multispectral, hyperspectral, and ultraspectral imagery X*], **5425**, 1–15, International Society for Optics and Photonics (2004).

[13] Hsuan, R. and Chein, I. C., "Automatic spectral target recognition in hyperspectral imagery," *IEEE Transactions on Aerospace and Electronic Systems* **39**(4), 1232–1249 (2003).

[14] Nascimento, J. M. P. and Dias, J. M. B., "Vertex component analysis: a fast algorithm to unmix hyperspectral data," *IEEE Transactions on Geoscience and Remote Sensing* **43**(4), 898–910 (2005).

[15] Wang, J. and Chang, C., "Applications of independent component analysis in endmember extraction and abundance quantification for hyperspectral imagery," *IEEE Transactions on Geoscience and Remote Sensing* **44**(9), 2601–2616 (2006).

[16] Gerg, I., "An evaluation of three endmember extraction algorithms: Atgp, ica-eea & vca," in [*2010 2nd Workshop on Hyperspectral Image and Signal Processing: Evolution in Remote Sensing*], 1–4 (2010).
[17] Kruse, F. A., "The spectral image processing system (sips)-interactive visualization and analysis of imaging spectrometer data," *Remote Sensing of Environment* **44**, 145–163 (1993).
[18] Chang, C.-I., "Spectral information divergence for hyperspectral image analysis," in [*IEEE 1999 International Geoscience and Remote Sensing Symposium. IGARSS'99 (Cat. No. 99CH36293)*], **1**, 509–511, IEEE (1999).
[19] Du, Y., Chang, C.-I., Ren, H., Chang, C.-C., Jensen, J. O., and D'Amico, F. M., "New hyperspectral discrimination measure for spectral characterization," *Optical Engineering* **43**(8), 1777–1787 (2004).
[20] Matheron, G., [*Random sets and integral geometry*], Wiley, New York, NY (1975).
[21] Serra, J., [*Image Analysis and Mathematical Morphology*], vol. 1, Academic press, New York (1982).
[22] Sternberg, S. R., "Grayscale morphology," *Computer Vision, Graphics, and Image Processing* **35**(3), 333–355 (1986).
[23] Heijmans, H., [*Morphological Image Operators*], Academic Press (1994).
[24] Soille, P., [*Morphological image analysis: principles and applications*], Springer Science & Business Media, 2 ed. (2013).
[25] Naegel, B., Passat, N., and Ronse, C., "Grey-level hit-or-miss transforms—part i: unified theory," *Pattern Recognition* **40**(2), 635–647 (2007).
[26] Weber, J. and Lefèvre, S., "A multivariate hit-or-miss transform for conjoint spatial and spectral template matching," *Image and Signal Processing*, 226–235, Springer Berlin Heidelberg (2008).
[27] Aptoula, E., Lefevre, S., and Ronse, C., "A hit-or-miss transform for multivariate images," *Pattern Recognition Letters* **30**(8), 760–764 (2009).
[28] Velasco-Forero, S. and Angulo, J., "Hit-or-miss transform in multivariate images," in [*International Conference on Advanced Concepts for Intelligent Vision Systems*], 452–463, Springer (2010).
[29] Weber, J. and Lefèvre, S., "Spatial and spectral morphological template matching," *Image and Vision Computing* **30**(12), 934–945 (2012).
[30] Lefèvre, S., Aptoula, E., Perret, B., and Weber, J., [*Morphological template matching in color images*], 241–277, Springer (2014).
[31] Ronse, C., "Why mathematical morphology needs complete lattices," *Signal Processing* **21**(2), 129–154 (1990).
[32] Barnett, V., "The ordering of multivariate data," *Journal of the Royal Statistical Society* **139**(3), 318–355 (1976).
[33] Hotelling, H., "Analysis of a complex of statistical variables into principal components," *Journal of educational psychology* **24**(6), 417 (1933).
[34] Murray, P., Marshall, S., and Bullinger, E., "The percentage occupancy hit or miss transform," in [*Signal Processing Conference, 2009 17th European*], 253–257, IEEE (2009).
[35] Gader, P., Zare, A., Close, R., Aitken, J., and Tuell, G., "Muufl gulfport hyperspectral and lidar airborne data set," (2013).
[36] Alvey, B., Zare, A., Cook, M., and Ho, D. K., "Adaptive coherence estimator (ace) for explosive hazard detection using wideband electromagnetic induction (wemi)," in [*Detection and Sensing of Mines, Explosive Objects, and Obscured Targets XXI*], **9823**, 982309, International Society for Optics and Photonics (2016).
[37] Zhu, L. and Wen, G., "Hyperspectral anomaly detection via background estimation and adaptive weighted sparse representation," *Remote Sensing* **10**(2), 272 (2018).
[38] Rao, D. A. and Guha, A., "Potential utility of spectral angle mapper and spectral information divergence methods for mapping lower vindhyan rocks and their accuracy assessment with respect to conventional lithological map in jharkhand, india," *Journal of the Indian Society of Remote Sensing* **46**(5), 737–747 (2018).
[39] Liu, W., Feng, X., Wang, S., Hu, B., Gan, Y., Zhang, X., and Lei, T., "Random selection-based adaptive saliency-weighted rxd anomaly detection for hyperspectral imagery," *International journal of remote sensing* **39**(8), 2139–2158 (2018).